Microscopic predictions for the production of neutron-rich nuclei in the reaction ^{176}Yb + ^{176}Yb

K. Godbey,[1,*] C. Simenel,[2,†] and A. S. Umar[1,‡]

[1]*Department of Physics and Astronomy, Vanderbilt University, Nashville, Tennessee 37235, USA*

[2]*Department of Theoretical Physics and Department of Nuclear Physics, Research School of Physics, The Australian National University, Canberra ACT 2601, Australia*

(Received 10 December 2019; accepted 19 February 2020; published 2 March 2020)

Background: Production of neutron-rich nuclei is of vital importance to both understanding nuclear structure far from stability and to informing astrophysical models of the rapid neutron capture process (r-process). Multinucleon transfer (MNT) in heavy-ion collisions offers a possibility to produce neutron-rich nuclei far from stability.

Purpose: The ^{176}Yb + ^{176}Yb reaction has been suggested as a potential candidate to explore the neutron-rich region surrounding the principal fragments. The current study has been conducted with the goal of providing guidance for future experiments wishing to study this (or similar) system.

Methods: Time-dependent Hartree-Fock (TDHF) and its time-dependent random-phase approximation (TDRPA) extension are used to examine both scattering and MNT characteristics in ^{176}Yb + ^{176}Yb. TDRPA calculations are performed to compute fluctuations and correlations of the neutron and proton numbers, allowing for estimates of primary fragment production probabilities.

Results: Both scattering results from TDHF and transfer results from the TDRPA are presented for different energies, orvientations, and impact parameters. In addition to fragment composition, scattering angles and total kinetic energies, as well as correlations between these observables are presented.

Conclusions: ^{176}Yb + ^{176}Yb appears to be an interesting probe for the midmass neutron-rich region of the chart of nuclides. The predictions of both TDHF and TDRPA are speculative, and will benefit from future experimental results to test the validity of this approach to studying MNT in heavy, symmetric collisions.

DOI: 10.1103/PhysRevC.101.034602

I. INTRODUCTION

The synthesis of neutron-rich nuclei is one of the most exciting and challenging tasks in both experimental and theoretical nuclear physics. From the lightest systems to the superheavy regime, knowledge about the nuclei at the extremes of the chart of nuclides is vital to understanding physical phenomena at multiple scales. At the foremost, neutron-rich nuclei are at the literal and figurative center of the rapid neutron capture process (r-process). Attempts at modeling the r-process utilize input from nuclear models to inform threshold energies for the reaction types that characterize this process [1]. Thus, strong theoretical understanding of both the static and dynamic properties of nuclei far from stability can give vital insight into the formation of stable heavy nuclei.

The production of neutron-rich nuclei is also of interest for studying nuclear structure, where exploring this region of the nuclear landscape clearly probes the edges of our current understanding of how finite nuclei form and are composed [2]. This includes studies of neutron-rich nuclei of all masses, ranging from oxygen [3] up to the superheavy element (SHE) region. SHEs are of particular note, as the formation and static properties of said nuclei have been the focus of many experimental [4–8] and theoretical [9–13] studies.

Over the years, many theoretical approaches to studying neutron-rich nuclei formation have been pursued for various reaction types. One such technique is to use models to study neutron enrichment via multinucleon transfer (MNT) in deep-inelastic collisions (DIC) and quasifission reactions [14–22]. While quasifission occurs at a much shorter time-scale than fusion-fission [23,24] and is the primary reaction mechanism that limits the formation of superheavy nuclei, the fragments produced may still be neutron-rich.

Quasifission reactions are often studied in asymmetric systems with, e.g., an actinide target [23,25–28]. However, quasifission can also be present in symmetric systems. In fact, the extreme case of quasifission in actinide-actinide collisions has been suggested as a possible reaction mechanism to obtain neutron-rich isotopes of high Z nuclei in particular as well as a possible means to search for SHE [29,30]. Theoretically, the investigation of collisions between very heavy nuclei has a rich history with various approaches, including the dinuclear system (DNS) model [31–38], relativistic mean-field (RMF) and Skyrme HF studies [39], reduced density-matrix formalism [40], Langevin equation [41–44], quantum molecular dynamics (QMD) [45], and improved quantum molecular dynamics (ImQMD) [20,46–49] calculations, as well as

*kyle.s.godbey@vanderbilt.edu
†cedric.simenel@anu.edu.au
‡umar@compsci.cas.vanderbilt.edu

time-dependent Hartree-Fock (TDHF) studies [17,19,50]. Over recent years, TDHF has proved to be a tool of choice to investigate fragment properties produced in various reactions, such as DIC [22,51], quasifission [21,28,47,52–57], and fission [58–67]. Recent reviews [68,69] succinctly summarize the current state of TDHF (and its extensions) as it has been applied to various MNT reactions.

In this work, we present a study of the $^{176}\mathrm{Yb} + {}^{176}\mathrm{Yb}$ system using TDHF and the time-dependent random phase approximation (TDRPA) [70–77] extension that considers the effect of one-body fluctuations around the TDHF trajectory. As discussed before, microscopic approaches such as TDHF and its extensions are commonly used in heavy-ion collision studies in different regions of the nuclear chart, positioning TDHF and TDRPA as tools of choice for the current investigation. Symmetric ^{176}Yb reactions were chosen because they are considered as a potential candidate to explore the neutron-rich region around the mass region $A \sim 170$–180 of the nuclear chart. The energies studied here correspond to beam energies of 7.5 and 10 MeV per nucleon. Calculations at 10 MeV/A have been performed to investigate the energy dependence of the results. The main results are discussed for the lower energy of 7.5 MeV/A, which is accessible with cyclotron beam facilities, such as, e.g., NSCL (US), Texas A&M, GANIL (France), and the superheavy element factory at Dubna. Specifically, an experimental investigation of this reaction are being considered in Dubna by Oganessian *et al.* and the work presented here was undertaken at their suggestion [78]. The base theory (TDHF) and the primary extension (TDRPA) are briefly described in Sec. II. Results for both scattering characteristics and transfer characteristics are discussed in Secs. III A and III B, respectively. A summary and outlook are then presented in Sec. IV.

II. FORMALISM: TDHF AND TDRPA

The TDHF theory provides a microscopic approach with which one may investigate a wide range of phenomena observed in low energy nuclear physics [68,69,79,80]. Specifically, TDHF provides a dynamic quantum many-body description of nuclear reactions in the vicinity of the Coulomb barrier, such as fusion [81–96] and transfer reactions [16,51,69,76,97–102].

The TDHF equations for the single-particle wave functions,

$$h(\{\phi_\mu\})\,\phi_\lambda(r,t) = i\hbar\frac{\partial}{\partial t}\phi_\lambda(r,t) \quad (\lambda = 1,\ldots,A)\,, \tag{1}$$

can be derived from a variational principle. The principal approximation in TDHF is that the many-body wave function $\Phi(t)$ is assumed to be a single time-dependent Slater determinant at all times. It describes the time-evolution of the single-particle wave functions in a mean-field corresponding to the dominant reaction channel. During the past decade it has become numerically feasible to perform TDHF calculations on a three-dimensional (3D) Cartesian grid without any symmetry restrictions and with much more accurate numerical methods [99,103–105].

The main limitation in the TDHF theory when studying features like particle transfer, however, is that it is optimized for the prediction of expectation values of one-body observables [106] and will under-predict fluctuations of those observables [107]. This is due to the fact that the fluctuation of one-body operators (such as the particle number operator) includes the expectation value of the square of a one-body operator,

$$\sigma_{XX} = \sqrt{\langle\hat{X}^2\rangle - \langle\hat{X}\rangle^2}\,, \tag{2}$$

that is outside the variational space of TDHF [106].

To obtain such quantities one needs to go beyond standard TDHF and consider the fluctuations around the TDHF mean-field trajectory using techniques like the stochastic mean-field theory (SMF) [108,109] or TDRPA [71]. Both of these approaches have been used to investigate MNT and fragment production [72–77,110–114].

Methods based on solving the Langevin equation on a potential energy surface, or those based on assuming a dinuclear system (DNS), are usually numerically much faster than fully microscopic approaches. Nevertheless, the increase of computational power and more efficient algorithms have enabled the use of microscopic codes to investigate MNT mechanisms even in the heaviest systems. Moreover, the main theoretical advantage of SMF and TDRPA methods in studying MNT is that they do not rely on empirical parameters and do not impose spatial restrictions on the single-particle wave functions.

In this work we follow a similar approach as in Refs. [76,77] to obtain particle number fluctuations and distributions about the outgoing fragments. The foundation of the method is to consider an alternate variational principle for generating the mean-field theory. In particular, the Balian-Vénéroni (BV) variational principle provides a powerful technique that optimizes the evaluation of expectation values for arbitrary operators [106]. When the operator chosen is a one-body operator, the method produces the TDHF equations exactly, suggesting that TDHF is the mean-field theory that is best suited for the calculation of one-body expectation values. However, as mentioned above, the calculation of fluctuations and correlations involves the square of a one-body operator. For TDHF alone, Eq. (2) results in the following expression for two generic operators $\hat{X}$ and $\hat{Y}$:

$$\sigma^2_{XY}(t_f) = \mathrm{Tr}\{Y\rho(t_f)X[I-\rho(t_f)]\}\,, \tag{3}$$

where I is the identity matrix and t_f is the final time. By utilizing the BV variational principle and extending the variational space to optimize for the expectation value of exponentials of one-body operators of the type $\exp(\varepsilon\hat{a}^\dagger\hat{a})$, one obtains an estimate of fluctuations and correlations in the limit of small ε [71]

$$\sigma^2_{XY}(t_f) = \lim_{\varepsilon\to 0}\frac{\mathrm{Tr}\{[\rho(t_i)-\rho_X(t_i,\varepsilon)][\rho(t_i)-\rho_Y(t_i,\varepsilon)]\}}{2\varepsilon^2} \tag{4}$$

which now depends on the one-body density matrices at the initial time t_i. Equation (4) also contains the density matrices $\rho_{X,Y}(t_i,\varepsilon)$ which have been transformed at t_f

according to $\rho_X(t_f,\varepsilon) = \exp(i\varepsilon X)\rho_X(t_f)\exp(-i\varepsilon X)$ and evolved back to t_i.

The procedure to compute Eq. (4) involves first transforming the states after the collision as

$$\tilde{\phi}^X_\alpha(r,t_f) = \exp[-i\varepsilon N_X \Theta_V(r)]\phi_\alpha(r,t_f), \tag{5}$$

where X stands for neutron (N), proton (Z), or total nucleon number (A). The operator N_X ensures that the transformation acts only on nucleons with the correct isospin with $N_A = 1$, $N_Z = \frac{1-\tau_3}{2}$, and $N_N = \frac{1+\tau_3}{2}$. The operator $\Theta_V(\hat{r})$ is a step function that is either 1 or 0 depending on whether r is within a volume of space, V, delimiting the fragment of interest. Finally, ε is a small number that is varied to achieve convergence.

These transformed states are then propagated backwards in time from the final time t_f to the initial time t_i. The trace in Eq. (4) can then be calculated, obtaining

$$\sigma_{XY} = \sqrt{\lim_{\varepsilon\to 0}\frac{\eta_{00}+\eta_{XY}-\eta_{0X}-\eta_{0Y}}{2\varepsilon^2}} \tag{6}$$

with η_{XY} describing the overlap between the states at time $t = t_i$,

$$\eta_{XY} = \sum_{\alpha\beta}\left|\langle\phi^X_\alpha(t_i)|\phi^Y_\beta(t_i)\rangle\right|^2. \tag{7}$$

In the case of $X, Y = 0$, this refers to states obtained with $\varepsilon = 0$ in Eq. (5). In principle, one should recover exactly the initial state as the evolution is unitary. However, using states that have been evolved forward and then backward in time with $\varepsilon = 0$ minimizes systematic errors from numerical inaccuracies [73,75].

The SLy4d parametrization of the Skyrme functional is used [115] and all calculations were performed in a numerical box with 66×66 points in the reaction plane, and 36 points along the axis perpendicular to the reaction plane. The grid spacing used was a standard 1.0 fm which provides an excellent numerical representation of spatial quantities using the basis spline collocation method [116]. For the TDRPA calculations, each initial orientation, energy, and impact parameter resulted in three additional TDHF evolutions (one for each X) for the time reversed evolution at one value of $\varepsilon = 2\times 10^{-3}$ in addition to occasionally scanning ε to ensure convergence of Eq. (6). In total, 200 full TDHF evolutions were required for the results presented in this work with each taking on the order of 10-55 h of wall time due to the large, three-dimensional box size chosen. This corresponds to roughly 250 d of computation time split among multiple nodes for the ^{176}Yb HF ground state configuration with a prolate deformation.

The proton and neutron numbers correlations and fluctuations computed with TDRPA are used to estimate probabilities for the formation of a given nuclide using Gaussian bivariate normal distributions of the form

$$\mathscr{P}(n,z) = \mathscr{P}(0,0)\exp\left[-\frac{1}{1-\rho^2}\left(\frac{n^2}{\sigma^2_{NN}}+\frac{z^2}{\sigma^2_{ZZ}}-\frac{2\rho nz}{\sigma_{NN}\sigma_{ZZ}}\right)\right], \tag{8}$$

where n and z are the number of transferred neutrons and protons, respectively. The correlations between N and Z are quantified by the parameter

$$\rho = \mathrm{sign}(\sigma_{NZ})\frac{\sigma^2_{NZ}}{\sigma_{NN}\sigma_{ZZ}} = \frac{\langle nz\rangle}{\sqrt{\langle n^2\rangle\langle z^2\rangle}}. \tag{9}$$

In principle, n and z could be very large and lead to unphysical predictions with fragments having, e.g., a negative number of protons and neutrons, or more nucleons than available. In practice, such spurious results could only happen for the most violent collisions where the fluctuations are large. To avoid such spurious effects, the probabilities are shifted so that $\mathscr{P}$ is zero when one fragment has all (or more) protons or neutrons. The resulting distribution is then normalized.

Although the ^{176}Yb nuclide is in a region where shape coexistence is often found [117–121], TDHF calculations can only be performed with one well-defined deformation (and orientation) of each collision partners in the entrance channel. In our calculations, the ground state is found to have a prolate deformation with $\beta_2 \simeq 0.33$ in its HF ground state. A higher energy oblate solution is also found with a difference of around 5 MeV in total binding energy. A set of calculations were also performed for the oblate solution, though the overall transfer behavior was found to be similar for both deformations despite the oblate one resulting in slightly lower fluctuations. In the following, we thus only show results for the prolate ground state.

This deformation allows for possible choices of the orientation of the nuclei. Extreme orientations are called "side" ("tip") when the deformation axis is initially perpendicular (parallel) to the collision axis. Although various intermediate orientations could be considered [56], we limit our study to tip-tip and side-side orientations where the initial orientations of both nuclei are identical. In addition to saving computational time, this restriction is necessary to ensure fully symmetric collisions and to avoid unphysical results in TDRPA [77].

Figure 1 shows the nucleus-nucleus potentials computed using the frozen Hartree-Fock (FHF) [85,122] and density-constrained frozen Hartree-Fock (DCFHF) [123] methods, respectively, neglecting and including the Pauli exclusion principle between the nucleons of different nuclei. Due to Pauli repulsion in DCFHF, the inner pocket potential is very shallow in the side-side configuration, and disappears in the tip-tip one. In this work, the effect of the orientation is studied by comparing tip-tip and side-side configurations at a center of mass energy $E_{\mathrm{c.m.}} = 660$ MeV. In addition, calculations are also performed at $E_{\mathrm{c.m.}} = 880$ MeV for both orientations to investigate the role of the energy on the reaction outcome.

III. RESULTS

In this section we present the results of TDHF and TDRPA studies of ^{176}Yb + ^{176}Yb reactions at different center of mass energies and initial orientations for a range of impact parameters. Both scattering features and particle number fluctuation derived quantities were calculated and are shown below.

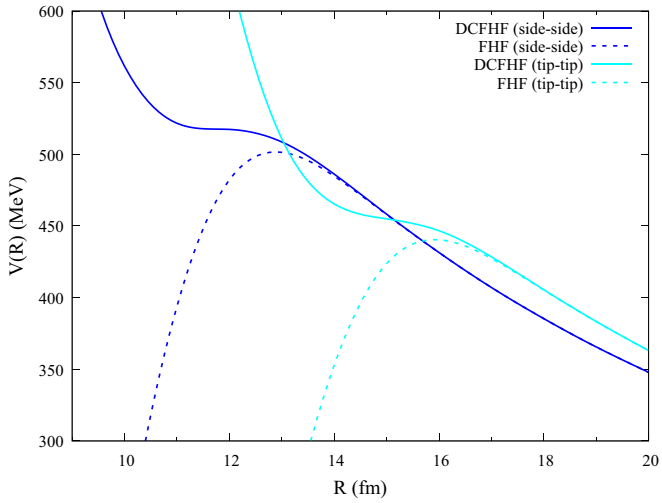

FIG. 1. Static nuclear potentials for ^{176}Yb + ^{176}Yb in the side-side [blue (dark) lines] and tip-tip [cyan (light) lines] orientations from FHF and DCFHF.

A. Scattering characteristics

The following section presents scattering results from the standard TDHF calculations of ^{176}Yb + ^{176}Yb collisions. The TDRPA extension to TDHF is not needed for these results, though this means the points can only be interpreted as the most likely outcome for each initial condition.

Scattering angles for the ^{176}Yb + ^{176}Yb system for both orientations are presented in Fig. 2. A similar deviation from Rutherford scattering is observed at impact parameters $b \leqslant 8$ fm for both orientations. These deviations are due to nuclear deflection and partial orbiting of the system. Note that no fusion is observed. The relatively flat shape of the curve around 50–60° at 660 MeV and 20–40° at 880 MeV implies a large number of events in these particular angular ranges.

The TKE of the outgoing fragments is plotted in Fig. 3 as a function of the impact parameter b for side-side collisions at the two center of mass energies. Although dissipation occurs at different impact parameter ranges ($b < 10$ fm at $E_{\text{c.m.}} = 660$ MeV and $b < 12$ fm at $E_{\text{c.m.}} = 880$ MeV), both curves exhibit similar behavior. In particular, the TKEs saturate at roughly the same energy (≈350–400 MeV) indicating full damping of the initial TKE for the most central collisions.

Among the mechanisms responsible for energy dissipation, nucleon transfer is expected to play an important role. Of course, in symmetric collisions the average number of nucleons in the fragments does not change. Nevertheless, multinucleon transfer is possible thanks to fluctuations, leading to finite widths in the fragment particle number distributions. These fluctuations are explored in the following section.

B. Transfer characteristics

This section focuses on the results obtained by extending TDHF to recover particle number fluctuations and correlations with the TDRPA.

Particle number fluctuations (σ_{ZZ} and σ_{NN}) and correlations (σ_{NZ}) calculated from Eq. (6) are shown in Fig. 4 as a

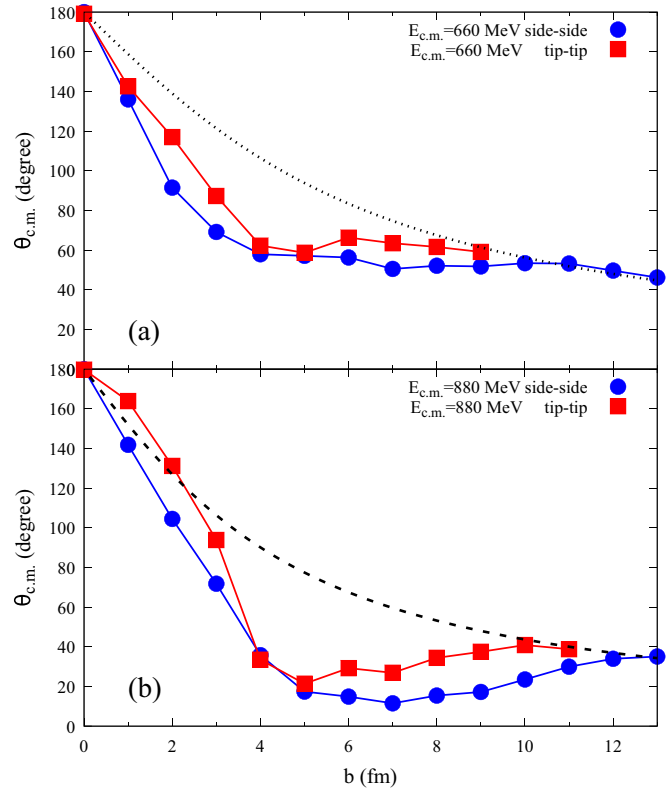

FIG. 2. Scattering angles for ^{176}Yb + ^{176}Yb collisions at center of mass energies (a) $E_{\text{c.m.}} = 660$ MeV and (b) $E_{\text{c.m.}} = 880$ MeV in the side-side (circles) and tip-tip (squares) orientations. The dotted (dashed) line plots the Rutherford scattering angle for $E_{\text{c.m.}} = 660$ MeV (880 MeV).

function of impact parameters for different initial conditions. The fluctuations are greater in general at the smaller impact parameters, though they do not converge to a single value. Similar variations in fluctuations were already observed in

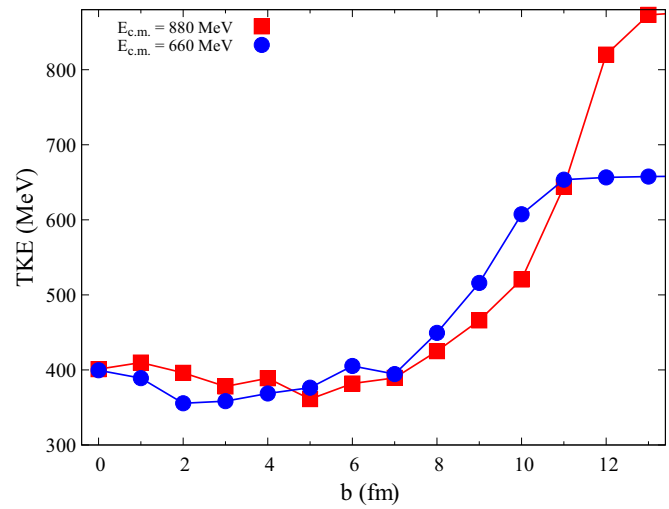

FIG. 3. Total kinetic energies of the outgoing fragments in ^{176}Yb + ^{176}Yb collisions at center of mass energies $E_{\text{c.m.}} = 660$ MeV (blue circles) and $E_{\text{c.m.}} = 880$ MeV (red squares) in the side-side orientation.

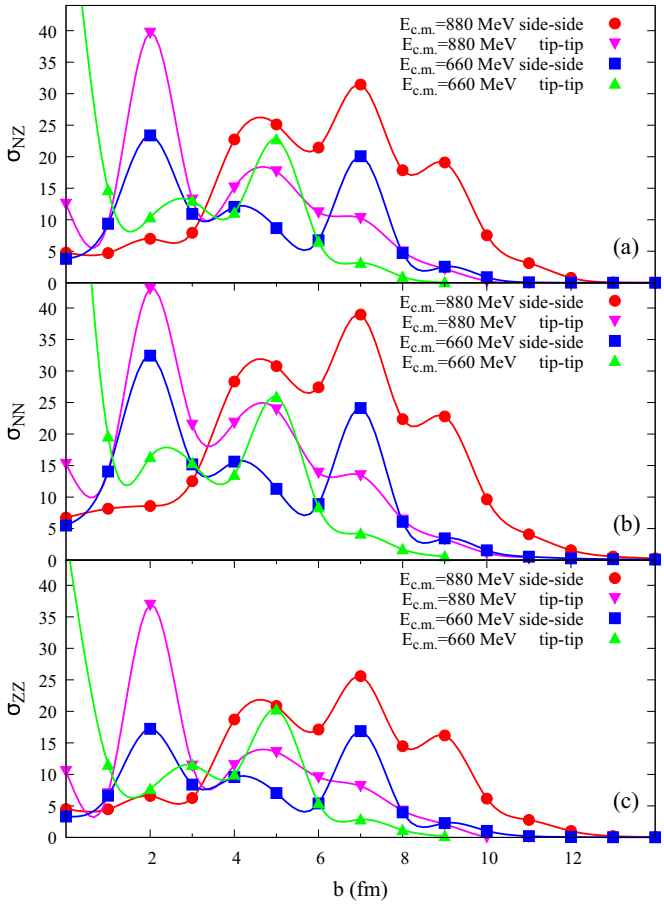

FIG. 4. TDRPA predictions of correlations σ_{NZ} (a) and fluctuations σ_{NN} (b) and σ_{ZZ} (c) for ^{176}Yb + ^{176}Yb collisions for four initial configurations over a range of impact parameters.

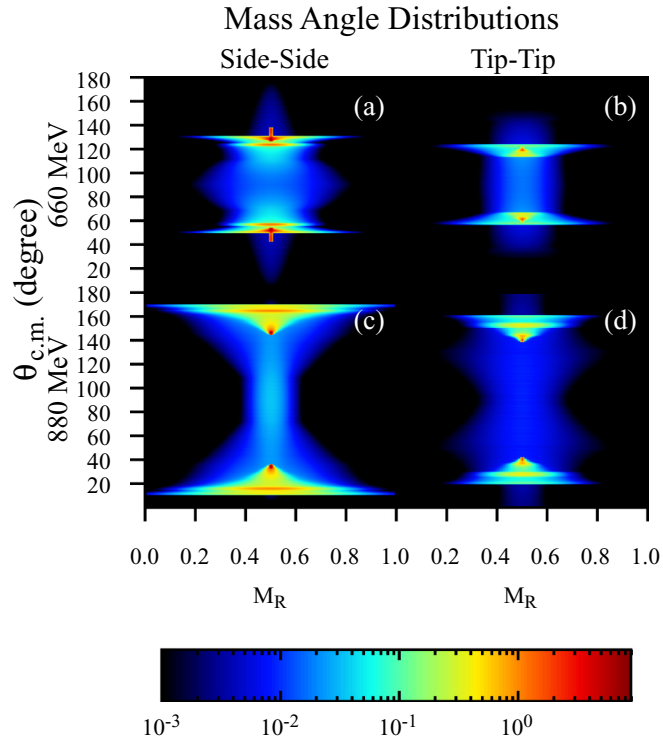

FIG. 5. Mass angle distributions for ^{176}Yb + ^{176}Yb collisions at (a) $E_{\text{c.m.}} = 660$ MeV in the side-side orientation, (b) $E_{\text{c.m.}} = 660$ MeV in the tip-tip orientation, (c) $E_{\text{c.m.}} = 880$ MeV in the side-side orientation, and (d) $E_{\text{c.m.}} = 880$ MeV in the tip-tip orientation. The color bar represents cross sections in mb per bin of mass ratio and degree.

earlier TDRPA studies of deep inelastic collisions in lighter systems [76,77]. Particularly large values are sometimes obtained, such as at 660 MeV in tip-tip central ($b = 0$) collisions, indicating approximately flat distributions around the TDHF average.

The three quantities, σ_{NZ}, σ_{NN}, and σ_{ZZ} exhibit very similar behaviors and are roughly proportional to each other. The neutron fluctuations are larger than the proton ones due to the larger number of neutrons involved. The fact that correlations and fluctuations behave similarly is due to the fact that the collisions are fully damped. Indeed, for less violent collisions such as quasi-elastic reactions, the correlations σ_{NZ} are much smaller than fluctuations [76]. In fact, the presence of positive correlations $\sigma_{NZ} > 0$ in deep inelastic collisions is a manifestation of the symmetry energy which favors a flow of protons and neutrons in the same direction, thus hindering the production of N/Z asymmetric fragments.

Fragment mass-angle distributions (MADs) are a standard tool used experimentally to interpret the dynamics of heavy-ion collisions [23,28,53,124–130]. Although TDHF has been used to help interpret theoretically these distributions [28,53,55,131], these earlier calculations only incorporate fluctuations coming from the distribution of initial conditions (e.g., different orientations). Here, we go beyond the mean-field prediction by including the fragment mass fluctuations from TDRPA. Note that we only include mass fluctuations, not fluctuations in scattering angle which are still determined solely by TDHF. Calculating quantum fluctuations of scattering angles is beyond the scope of this work, although they might be necessary for a more detailed comparison with experimental MADs.

The resulting MADs for ^{176}Yb + ^{176}Yb reactions are shown in Fig. 5. The mass ratio M_R is defined as the ratio of the fragment mass over the total mass of the system. The distributions of mass ratios are determined assuming Gaussian distributions with standard deviation $\sigma_{M_R} = \sigma_{AA}/A$, limited and normalized to the physical region $0 \leqslant M_R \leqslant 1$ (see Sec. II). There is then an M_R distribution per initial condition (defined by $E_{\text{c.m.}}$, b, and the orientations), but only a single scattering angle $\theta_{\text{c.m.}}$. To obtain a continuous representation of the scattering angle, $\theta_{\text{c.m.}}$ is discretized into bins of $\Delta\theta = 1$ degree and interpolated between the values obtained by TDHF.

The figures are symmetric about 90° as both outgoing fragments are identically the same and will then travel outwards at complimentary angles. Specific orientations such as side-side and tip-tip will not be accessible in an experimental setting of course. Interestingly, when investigating initial energy dependence of the MAD [compare panels (a) and (c), (b) and (d) in Fig. 5], it can be seen that different outgoing angles are preferred depending on the incoming center of mass

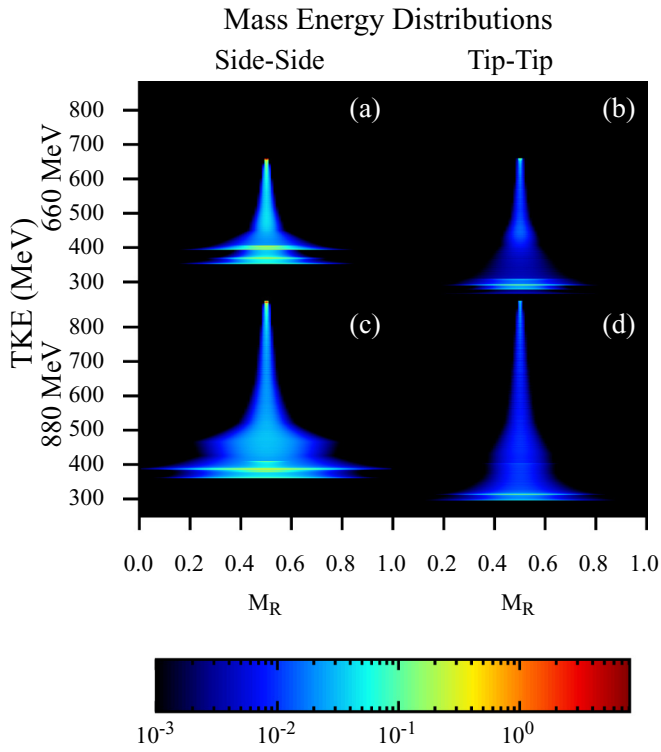

FIG. 6. Mass energy distributions for ^{176}Yb + ^{176}Yb collisions at (a) $E_{\text{c.m.}} = 660$ MeV in the side-side orientation, (b) $E_{\text{c.m.}} = 660$ MeV in the tip-tip orientation, (c) $E_{\text{c.m.}} = 880$ MeV in the side-side orientation, and (d) $E_{\text{c.m.}} = 880$ MeV in the tip-tip orientation. The color bar represents cross sections in mb per bin of mass ratio and MeV.

energy with back (and forward) scattering events being more prevalent in the higher energy regime.

This agrees well with what is seen in Fig. 2, where many impact parameters result in scattering angles around 50–60 degrees at $E_{\text{c.m.}} = 660$ MeV and around 20–40 degrees at 880 MeV. This is the case for both tip-tip and side-side orientations, though the tip-tip results tend further towards the intermediate angles than side-side at the same energy.

While the predictive capability of this method needs to be compared with experimental results and tested, this suggests a strong energy dependence and that detection of fragment production will greatly benefit from large angle detectors. The energy dependence seen in the MAD is not intuitive, and may prove to be useful for informing experimental setups.

Useful information can also be obtained from the correlations between fragment mass and kinetic energy [27,133–136]. Figure 6 presents mass energy distributions (MED) that detail the predicted TKE of outgoing fragments. It should be noted here that, while the theory provides particle number fluctuations, the values for TKE are single points (as in the case of $\theta_{\text{c.m.}}$) as predicted by TDHF alone. That is, widths of the TKE distributions are currently unknown with the method used here. This would make for an excellent extension to the theory, bringing it more in line with what can be experimentally observed.

The MEDs exhibit a continuous broadening of the mass distribution with increasing energy dissipation. The saturation

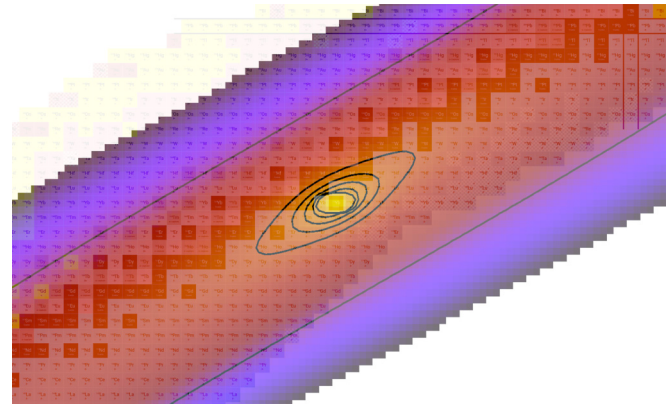

FIG. 7. Primary fragments production cross sections for ^{176}Yb + ^{176}Yb collisions at $E_{\text{c.m.}} = 660$ MeV in the side-side orientation overlaid onto the chart of nuclides. The innermost contour corresponds to a cross section of 1 mb, with subsequent contours drawn every 0.2 mb. Finally, we also plot a boundary contour drawn at the microbarn level. Chart from [132].

of TKE lies around 350–400 MeV for side-side collisions (see also Fig. 3) and around 250–300 MeV for tip-tip. This difference between orientations is interesting as it indicates a larger kinetic energy dissipation with less compact configurations. A possible explanation is that the nuclei overlap at a larger distance in the tip-tip configuration, thus producing energy dissipation earlier in the collision process than in the side-side orientation.

In general, the MEDs show peaks around the elastic and fully damped regions which results from the large range of impact parameters contributing to both mechanisms.

C. Primary fragments production

Using the correlations and fluctuations shown in Fig. 4, a map of probabilities can be made in the N-Z plane assuming a modified Gaussian bivariate normal distribution [see Sec. II and Eq. (8)]. This choice of using a Gaussian is the primary assumption when calculating probabilities and related quantities and may not accurately describe the true distribution far from the center.

These probability distributions at multiple impact parameters can then be integrated over to produce a map of primary fragment production cross sections which is presented in Fig. 7 overlaid atop a section of the chart of nuclides in the region surrounding ^{176}Yb [132]. As the probability distributions for each impact parameter will be centered around the ^{176}Yb ($Z = 70, N = 106$) nuclide, the resulting cross sections are also symmetric about ^{176}Yb. The inclusion of correlations between protons and neutrons via σ_{NZ} more or less aligns the distribution parallel to the valley of stability due to the symmetry energy.

Subsequent decay of the fragments would inevitably bring the final products closer to the valley of stability. Here, our focus is on primary fragment productions and the prediction of evaporation residue cross-sections are beyond the scope of this work. In fact, experimental measurements of mass-angle distributions using time of flight techniques are for primary

fragments as they assume two-body kinematics [137]. To estimate the evaporation residue cross sections would require to first compute the excitation energy of the fragments and then predict their decay with a statistical model [51,138].

One way to minimize evaporation is to consider less violent collisions. In terms of primary fragment productions, 660 and 880 MeV center of mass energies are quite similar (this can be seen by the relatively similar particle number fluctuations in Fig. 4). However, the higher energy will lead to more neutron evaporation and thus to less exotic evaporation residues. Use of relatively neutron-rich ^{176}Yb nuclei in symmetric collisions may then allow for this reaction to act as a probe of the neutron-rich region surrounding the principal outgoing fragment.

IV. SUMMARY AND DISCUSSION

Multiple TDHF and TDRPA calculations have been performed for the $^{176}\mathrm{Yb} + {}^{176}\mathrm{Yb}$ system with various initial orientations, energies, and impact parameters. Standard TDHF allows for the classification of general scattering characteristics, while the TDRPA technique extends the approach to include correlations and fluctuations of particle numbers of the reaction fragments. This extension provides a theoretical framework that more closely resembles what will be seen in experimental investigations of this (and similar) systems.

In examining figures such as the mass-angle distributions in Fig. 5, information regarding the angular distribution of fragments can be gleaned and suggest large acceptance detectors to maximize measurement capability. Mass-energy distributions shown in Fig. 6 are also useful to investigate, e.g., the interplay between dissipation and fluctuations. In both cases, however, fluctuations of $\theta_{\mathrm{c.m.}}$ and of TKE are not predicted in the present study. The latter would require new implementations of the TDRPA to these observables, or the use of alternative approaches such as the stochastic mean-field theory [64] or an extension of the Langevin equation [139]. Both methods have been recently used to investigate kinetic energy distributions in fission fragments. In order to benchmark our theoretical methods as applied to symmetric heavy nuclei, all predictions presented in this study would greatly benefit from experimental verification.

The methods used here provide a very powerful tool for investigating symmetric systems, though an important caveat should be discussed regarding the interpretation of these results. TDRPA produces only correlations and fluctuations, not the actual distributions themselves, which are then taken to be of a Gaussian nature. This assumption may break down when far from the center of the distribution or if the shape at the center itself is too flat and deviates sufficiently from a Gaussian behavior. It is then extremely important to compare with observations made in experimental studies such that we may better understand how to interpret the results coming from these methods.

Regardless, the $^{176}\mathrm{Yb} + {}^{176}\mathrm{Yb}$ system presents itself as a viable candidate for studies of MNT processes and production of neutron rich nuclei in the region around $A \approx 176$. The map of possible primary fragments loosely painted in Fig. 7 presents an exciting range of previously inaccessible nuclei, with the above caveat applying the further one goes from the center of the distribution. Another caveat is that the predicted distribution is for primary fragments only and that statistical decay should be included in order to predict fragment produced after evaporation, e.g., following [22,51,138].

ACKNOWLEDGMENTS

We thank Yu. Ts. Oganessian and D. J. Hinde for stimulating discussions. This work has been supported by the US Department of Energy under Grant No. DE-SC0013847 with Vanderbilt University and by the Australian Research Councils Grant No. DP190100256.

[1] J. J. Cowan, C. Sneden, J. E. Lawler, A. Aprahamian, M. Wiescher, K. Langanke, G. Martínez-Pinedo, and F.-K. Thielemann, Making the heaviest elements in the universe: A review of the rapid neutron capture process, arXiv:1901.01410.

[2] T. Otsuka, A. Gade, O. Sorlin, T. Suzuki, and Y. Utsuno, Evolution of nuclear structure in exotic nuclei driven by nuclear forces, arXiv:1805.06501 [Rev. Mod. Phys. (to be published)].

[3] R. T. deSouza, S. Hudan, V. E. Oberacker, and A. S. Umar, Confronting measured near- and sub-barrier fusion cross sections for $^{20}\mathrm{O} + {}^{12}\mathrm{C}$ with a microscopic method, Phys. Rev. C **88**, 014602 (2013).

[4] S. Hofmann, F. P. Heßberger, D. Ackermann, G. Münzenberg, S. Antalic, P. Cagarda, B. Kindler, J. Kojouharova, M. Leino, B. Lommel, R. Mann, A. G. Popeko, S. Reshitko, S. Śaro, J. Uusitalo, and A. V. Yeremin, New results on elements 111 and 112, Eur. Phys. J. A **14**, 147 (2002).

[5] G. Münzenberg and K. Morita, Synthesis of the heaviest nuclei in cold fusion reactions, Nucl. Phys. A **944**, 3 (2015).

[6] K. Morita, SHE research at RIKEN/GARIS, Nucl. Phys. A **944**, 30 (2015).

[7] Yu. Ts. Oganessian and V. K. Utyonkov, Superheavy nuclei from ^{48}Ca-induced reactions, Nucl. Phys. A **944**, 62 (2015).

[8] J. B. Roberto, C. W. Alexander, R. A. Boll, J. D. Burns, J. G. Ezold, L. K. Felker, S. L. Hogle, and K. P. Rykaczewski, Actinide targets for the synthesis of super-heavy elements, Nucl. Phys. A **944**, 99 (2015).

[9] M. Bender, K. Rutz, P.-G. Reinhard, J. A. Maruhn, and W. Greiner, Shell structure of superheavy nuclei in self-consistent mean-field models, Phys. Rev. C **60**, 034304 (1999).

[10] W. Nazarewicz, M. Bender, S. Ćwiok, P. H. Heenen, A. T. Kruppa, P.-G. Reinhard, and T. Vertse, Theoretical description of superheavy nuclei, Nucl. Phys. A **701**, 165 (2002).

[11] S. Ćwiok, P.-H. Heenen, and W. Nazarewicz, Shape coexistence and triaxiality in the superheavy nuclei, Nature **433**, 705 (2005).

[12] J. C. Pei, W. Nazarewicz, J. A. Sheikh, and A. K. Kerman, Fission Barriers of Compound Superheavy Nuclei, Phys. Rev. Lett. **102**, 192501 (2009).

[13] J. R. Stone, K. Morita, P. A. M. Guichon, and A. W. Thomas, Physics of even-even superheavy nuclei with $96 < Z < 110$ in the quark-meson-coupling model, Phys. Rev. C **100**, 044302 (2019).

[14] G. G. Adamian, N. V. Antonenko, and W. Scheid, Characteristics of quasifission products within the dinuclear system model, Phys. Rev. C **68**, 034601 (2003).

[15] V. Zagrebaev and W. Greiner, Shell effects in damped collisions: A new way to superheavies, J. Phys. G **34**, 2265 (2007).

[16] A. S. Umar, V. E. Oberacker, and J. A. Maruhn, Neutron transfer dynamics and doorway to fusion in time-dependent Hartree-Fock theory, Eur. Phys. J. A **37**, 245 (2008).

[17] C. Golabek and C. Simenel, Collision Dynamics of two ^{238}U Atomic Nuclei, Phys. Rev. Lett. **103**, 042701 (2009).

[18] Y. Aritomo, Analysis of dynamical processes using the mass distribution of fission fragments in heavy-ion reactions, Phys. Rev. C **80**, 064604 (2009).

[19] D. J. Kedziora and C. Simenel, New inverse quasifission mechanism to produce neutron-rich transfermium nuclei, Phys. Rev. C **81**, 044613 (2010).

[20] K. Zhao, Z. Li, Y. Zhang, N. Wang, Q. Li, C. Shen, Y. Wang, and X. Wu, Production of unknown neutron-rich isotopes in $^{238}\mathrm{U} + {}^{238}\mathrm{U}$ collisions at near-barrier energy, Phys. Rev. C **94**, 024601 (2016).

[21] K. Sekizawa, Enhanced nucleon transfer in tip collisions of $^{238}\mathrm{U} + {}^{124}\mathrm{Sn}$, Phys. Rev. C **96**, 041601(R) (2017).

[22] Z. Wu and L. Guo, Microscopic studies of production cross sections in multinucleon transfer reaction $^{58}\mathrm{Ni} + {}^{124}\mathrm{Sn}$, Phys. Rev. C **100**, 014612 (2019).

[23] J. Tõke, R. Bock, G. X. Dai, A. Gobbi, S. Gralla, K. D. Hildenbrand, J. Kuzminski, W. F. J. Müller, A. Olmi, H. Stelzer, B. B. Back, and S. Bjørnholm, Quasi-fission: The mass-drift mode in heavy-ion reactions, Nucl. Phys. A **440**, 327 (1985).

[24] R. du Rietz, D. J. Hinde, M. Dasgupta, R. G. Thomas, L. R. Gasques, M. Evers, N. Lobanov, and A. Wakhle, Predominant Time Scales in Fission Processes in Reactions of S, Ti and Ni with W: Zeptosecond Versus Attosecond, Phys. Rev. Lett. **106**, 052701 (2011).

[25] D. J. Hinde, D. Hilscher, H. Rossner, B. Gebauer, M. Lehmann, and M. Wilpert, Neutron emission as a probe of fusion-fission and quasi-fission dynamics, Phys. Rev. C **45**, 1229 (1992).

[26] D. J. Hinde, M. Dasgupta, J. R. Leigh, J. P. Lestone, J. C. Mein, C. R. Morton, J. O. Newton, and H. Timmers, Fusion-Fission Versus Quasifission: Effect of Nuclear Orientation, Phys. Rev. Lett. **74**, 1295 (1995).

[27] M. G. Itkis, J. Äystö, S. Beghini, A. A. Bogachev, L. Corradi, O. Dorvaux, A. Gadea, G. Giardina, F. Hanappe, I. M. Itkis, M. Jandel, J. Kliman, S. V. Khlebnikov, G. N. Kniajeva, N. A. Kondratiev, E. M. Kozulin, L. Krupa, A. Latina, T. Materna, G. Montagnoli, Yu. Ts. Oganessian, I. V. Pokrovsky, E. V. Prokhorova, N. Rowley, V. A. Rubchenya, A. Ya. Rusanov, R. N. Sagaidak, F. Scarlassara, A. M. Stefanini, L. Stuttge, S. Szilner, M. Trotta, W. H. Trzaska, D. N. Vakhtin, A. M. Vinodkumar, V. M. Voskressenski, and V. I. Zagrebaev, Shell effects in fission and quasi-fission of heavy and superheavy nuclei, Nucl. Phys. A **734**, 136 (2004).

[28] A. Wakhle, C. Simenel, D. J. Hinde, M. Dasgupta, M. Evers, D. H. Luong, R. du Rietz, and E. Williams, Interplay Between Quantum Shells and Orientation in Quasifission, Phys. Rev. Lett. **113**, 182502 (2014).

[29] Z. Majka, R. Płaneta, Z. Sosin, A. Wieloch, K. Zelga, M. Adamczyk, K. Pelczar, M. Barbui, S. Wuenschel, K. Hagel, X. Cao, E.-J. Kim, J. Natowitz, R. Wada, H. Zheng, G. Giuliani, and S. Kowalski, A novel experimental setup for rare events selection and its potential application to super-heavy elements search, Acta Phys. Pol. B **49**, 1801 (2018).

[30] S. Wuenschel, K. Hagel, M. Barbui, J. Gauthier, X. G. Cao, R. Wada, E. J. Kim, Z. Majka, R. Płaneta, Z. Sosin, A. Wieloch, K. Zelga, S. Kowalski, K. Schmidt, C. Ma, G. Zhang, and J. B. Natowitz, Experimental survey of the production of α-decaying heavy elements in $^{238}\mathrm{U} + {}^{232}\mathrm{Th}$ reactions at 7.5–6.1 MeV/nucleon, Phys. Rev. C **97**, 064602 (2018).

[31] Y. E. Penionzhkevich, G. G. Adamian, and N. V. Antonenko, Towards neutron drip line via transfer-type reactions, Phys. Lett. B **621**, 119 (2005).

[32] G. G. Adamian, N. V. Antonenko, S. M. Lukyanov, and Y. E. Penionzhkevich, Possibility of production of neutron-rich isotopes in transfer-type reactions at intermediate energies, Phys. Rev. C **78**, 024613 (2008).

[33] Z.-Q. Feng, G.-M. Jin, and J.-Q. Li, Production of heavy isotopes in transfer reactions by collisions of $^{238}\mathrm{U} + {}^{238}\mathrm{U}$, Phys. Rev. C **80**, 067601 (2009).

[34] G. G. Adamian, N. V. Antonenko, V. V. Sargsyan, and W. Scheid, Possibility of production of neutron-rich Zn and Ge isotopes in multinucleon transfer reactions at low energies, Phys. Rev. C **81**, 024604 (2010).

[35] G. G. Adamian, N. V. Antonenko, and D. Lacroix, Production of neutron-rich Ca, Sn, and Xe isotopes in transfer-type reactions with radioactive beams, Phys. Rev. C **82**, 064611 (2010).

[36] Z.-Q. Feng, Production of neutron-rich isotopes around $N = 126$ in multinucleon transfer reactions, Phys. Rev. C **95**, 024615 (2017).

[37] L. Zhu, J. Su, W.-J. Xie, and F.-S. Zhang, Theoretical study on production of heavy neutron-rich isotopes around the N=126 shell closure in radioactive beam induced transfer reactions, Phys. Lett. B **767**, 437 (2017).

[38] X. J. Bao, S. Q. Guo, J. Q. Li, and H. F. Zhang, Influence of neutron excess of projectile on multinucleon transfer reactions, Phys. Lett. B **785**, 221 (2018).

[39] R. K. Gupta, S. K. Patra, P. D. Stevenson, and W. Greiner, A highly neutron–rich cluster and/or a superheavy nucleus in the compound nucleus $^{238}\mathrm{U} + {}^{238}\mathrm{U}$: A mean field study, Int. J. Mod. Phys. E **16**, 1721 (2007).

[40] V. V. Sargsyan, Z. Kanokov, G. G. Adamian, N. V. Antonenko, and W. Scheid, Interaction times in the $^{136}\mathrm{Xe} + {}^{136}\mathrm{Xe}$ and $^{238}\mathrm{U} + {}^{238}\mathrm{U}$ reactions with a quantum master equation, Phys. Rev. C **80**, 047603 (2009).

[41] V. I. Zagrebaev, Yu. Ts. Oganessian, M. G. Itkis, and W. Greiner, Superheavy nuclei and quasi-atoms produced in collisions of transuranium ions, Phys. Rev. C **73**, 031602(R) (2006).

[42] V. Zagrebaev and W. Greiner, New way for the production of heavy neutron-rich nuclei, J. Phys. G **35**, 125103 (2008).

[43] A. V. Karpov and V. V. Saiko, Modeling near-barrier collisions of heavy ions based on a Langevin-type approach, Phys. Rev. C **96**, 024618 (2017).

[44] V. V. Saiko and A. V. Karpov, Analysis of multinucleon transfer reactions with spherical and statically deformed nuclei using a Langevin-type approach, Phys. Rev. C **99**, 014613 (2019).

[45] K. Zhao, X. Wu, and Z. Li, Quantum molecular dynamics study of the mass distribution of products in 7.0*A* MeV ^{238}U + ^{238}U collisions, Phys. Rev. C **80**, 054607 (2009).

[46] J. Tian, X. Wu, K. Zhao, Y. Zhang, and Z. Li, Properties of the composite systems formed in the reactions ^{238}U + ^{238}U and ^{232}Th + ^{250}Cf, Phys. Rev. C **77**, 064603 (2008).

[47] N. Wang and L. Guo, New neutron-rich isotope production in ^{154}Sm + ^{160}Gd, Phys. Lett. B **760**, 236 (2016).

[48] H. Yao and N. Wang, Microscopic dynamics simulations of multinucleon transfer in ^{86}Kr + ^{64}Ni at 25 MeV/nucleon, Phys. Rev. C **95**, 014607 (2017).

[49] C. Li, P. Wen, J. Li, G. Zhang, B. Li, X. Xu, Z. Liu, S. Zhu, and F.-S. Zhang, Production mechanism of new neutron-rich heavy nuclei in the ^{136}Xe + ^{198}Pt reaction, Phys. Lett. B **776**, 278 (2018).

[50] R. Y. Cusson, J. A. Maruhn, and H. Stöcker, Collision of ^{238}U + ^{238}U using a three–dimensional TDHF–BCS model, Z. Phys. A **294**, 257 (1980).

[51] A. S. Umar, C. Simenel, and W. Ye, Transport properties of isospin asymmetric nuclear matter using the time-dependent Hartree-Fock method, Phys. Rev. C **96**, 024625 (2017).

[52] V. E. Oberacker, A. S. Umar, and C. Simenel, Dissipative dynamics in quasifission, Phys. Rev. C **90**, 054605 (2014).

[53] K. Hammerton, Z. Kohley, D. J. Hinde, M. Dasgupta, A. Wakhle, E. Williams, V. E. Oberacker, A. S. Umar, I. P. Carter, K. J. Cook, J. Greene, D. Y. Jeung, D. H. Luong, S. D. McNeil, C. S. Palshetkar, D. C. Rafferty, C. Simenel, and K. Stiefel, Reduced quasifission competition in fusion reactions forming neutron-rich heavy elements, Phys. Rev. C **91**, 041602(R) (2015).

[54] A. S. Umar and V. E. Oberacker, Time-dependent HF approach to SHE dynamics, Nucl. Phys. A **944**, 238 (2015).

[55] A. S. Umar, V. E. Oberacker, and C. Simenel, Fusion and quasifission dynamics in the reactions ^{48}Ca + ^{249}Bk and ^{50}Ti + ^{249}Bk using a time-dependent Hartree-Fock approach, Phys. Rev. C **94**, 024605 (2016).

[56] K. Godbey, A. S. Umar, and C. Simenel, Deformed shell effects in ^{48}Ca + ^{249}Bk quasifission fragments, Phys. Rev. C **100**, 024610 (2019).

[57] X. Jiang and N. Wang, Probing the production mechanism of neutron-rich nuclei in multinucleon transfer reactions, Phys. Rev. C **101**, 014604 (2020).

[58] C. Simenel and A. S. Umar, Formation and dynamics of fission fragments, Phys. Rev. C **89**, 031601(R) (2014).

[59] G. Scamps, C. Simenel, and D. Lacroix, Superfluid dynamics of ^{258}Fm fission, Phys. Rev. C **92**, 011602(R) (2015).

[60] P. M. Goddard, P. D. Stevenson, and A. Rios, Fission dynamics within time-dependent Hartree-Fock: deformation-induced fission, Phys. Rev. C **92**, 054610 (2015).

[61] Y. Tanimura, D. Lacroix, and G. Scamps, Collective aspects deduced from time-dependent microscopic mean-field with pairing: Application to the fission process, Phys. Rev. C **92**, 034601 (2015).

[62] P. M. Goddard, P. D. Stevenson, and A. Rios, Fission dynamics within time-dependent Hartree-Fock. II. Boost-induced fission, Phys. Rev. C **93**, 014620 (2016).

[63] A. Bulgac, P. Magierski, K. J. Roche, and I. Stetcu, Induced Fission of ^{240}Pu within a Real-Time Microscopic Framework, Phys. Rev. Lett. **116**, 122504 (2016).

[64] Y. Tanimura, D. Lacroix, and S. Ayik, Microscopic Phase–Space Exploration Modeling of ^{258}Fm Spontaneous Fission, Phys. Rev. Lett. **118**, 152501 (2017).

[65] G. Scamps and C. Simenel, Impact of pear-shaped fission fragments on mass-asymmetric fission in actinides, Nature **564**, 382 (2018).

[66] A. Bulgac, S. Jin, K. J. Roche, N. Schunck, and I. Stetcu, Fission dynamics of ^{240}Pu from saddle to scission and beyond, Phys. Rev. C **100**, 034615 (2019).

[67] G. Scamps and C. Simenel, Effect of shell structure on the fission of sub-lead nuclei, Phys. Rev. C **100**, 041602(R) (2019).

[68] C. Simenel and A. S. Umar, Heavy-ion collisions and fission dynamics with the time–dependent Hartree-Fock theory and its extensions, Prog. Part. Nucl. Phys. **103**, 19 (2018).

[69] K. Sekizawa, TDHF theory and its extensions for the multinucleon transfer reaction: A mini review, Front. Phys. **7**, 20 (2019).

[70] P.-G. Reinhard, K. Goeke, and R. Y. Cusson, A time dependent RPA-theory for heavy ion reactions, Z. Phys. A **295**, 45 (1980).

[71] R. Balian and M. Véneroni, Fluctuations in a time-dependent mean-field approach, Phys. Lett. B **136**, 301 (1984).

[72] J. B. Marston and S. E. Koonin, Mean-Field Calculations of Fluctuations in Nuclear Collisions, Phys. Rev. Lett. **54**, 1139 (1985).

[73] P. Bonche and H. Flocard, Dispersion of one-body operators with the Balian-Veneroni variational principle, Nucl. Phys. A **437**, 189 (1985).

[74] J. M. A. Broomfield and P. D. Stevenson, Mass dispersions from giant dipole resonances using the Balian-Véneroni variational approach, J. Phys. G **35**, 095102 (2008).

[75] J. M. A. Broomfield, Calculations of Mass Distributions using the Balian-Véneroni Variational Approach, Ph.D. thesis, University of Surrey, Guildford, United Kingdom (2009).

[76] C. Simenel, Particle-Number Fluctuations and Correlations in Transfer Reactions Obtained Using the Balian-Véneroni Variational Principle, Phys. Rev. Lett. **106**, 112502 (2011).

[77] E. Williams, K. Sekizawa, D. J. Hinde, C. Simenel, M. Dasgupta, I. P. Carter, K. J. Cook, D. Y. Jeung, S. D. McNeil, C. S. Palshetkar, D. C. Rafferty, K. Ramachandran, and A. Wakhle, Exploring Zeptosecond Quantum Equilibration Dynamics: From Deep-Inelastic to Fusion-Fission Outcomes in ^{58}Ni + ^{60}Ni Reactions, Phys. Rev. Lett. **120**, 022501 (2018).

[78] Yu. Ts. Oganessian, private communication (2018).

[79] J. W. Negele, The mean-field theory of nuclear-structure and dynamics, Rev. Mod. Phys. **54**, 913 (1982).

[80] C. Simenel, Nuclear quantum many-body dynamics, Eur. Phys. J. A **48**, 152 (2012).

[81] P. Bonche, B. Grammaticos, and S. Koonin, Three-dimensional time-dependent Hartree-Fock calculations of ^{16}O + ^{16}O and ^{40}Ca + ^{40}Ca fusion cross sections, Phys. Rev. C **17**, 1700 (1978).

[82] H. Flocard, S. E. Koonin, and M. S. Weiss, Three-dimensional time-dependent Hartree-Fock calculations: Application to ^{16}O + ^{16}O collisions, Phys. Rev. C **17**, 1682 (1978).

[83] C. Simenel, P. Chomaz, and G. de France, Quantum Calculation of the Dipole Excitation in Fusion Reactions, Phys. Rev. Lett. **86**, 2971 (2001).

[84] A. S. Umar and V. E. Oberacker, Time dependent Hartree-Fock fusion calculations for spherical, deformed systems, Phys. Rev. C **74**, 024606 (2006).

[85] K. Washiyama and D. Lacroix, Energy dependence of the nucleus-nucleus potential close to the Coulomb barrier, Phys. Rev. C **78**, 024610 (2008).

[86] A. S. Umar, V. E. Oberacker, J. A. Maruhn, and P.-G. Reinhard, Entrance channel dynamics of hot and cold fusion reactions leading to superheavy elements, Phys. Rev. C **81**, 064607 (2010).

[87] A. S. Umar, V. E. Oberacker, J. A. Maruhn, and P.-G. Reinhard, Microscopic calculation of precompound excitation energies for heavy-ion collisions, Phys. Rev. C **80**, 041601(R) (2009).

[88] L. Guo and T. Nakatsukasa, Time-dependent Hartree-Fock studies of the dynamical fusion threshold, EPJ Web Conf. **38**, 09003 (2012).

[89] R. Keser, A. S. Umar, and V. E. Oberacker, Microscopic study of Ca + Ca fusion, Phys. Rev. C **85**, 044606 (2012).

[90] C. Simenel, R. Keser, A. S. Umar, and V. E. Oberacker, Microscopic study of ^{16}O + ^{16}O fusion, Phys. Rev. C **88**, 024617 (2013).

[91] V. E. Oberacker, A. S. Umar, J. A. Maruhn, and P.-G. Reinhard, Dynamic microscopic study of pre-equilibrium giant resonance excitation and fusion in the reactions ^{132}Sn + ^{48}Ca and ^{124}Sn + ^{40}Ca, Phys. Rev. C **85**, 034609 (2012).

[92] V. E. Oberacker, A. S. Umar, J. A. Maruhn, and P. G. Reinhard, Microscopic study of the ^{132,124}Sn + ^{96}Zr reactions: Dynamic excitation energy, energy-dependent heavy-ion potential, and capture cross section, Phys. Rev. C **82**, 034603 (2010).

[93] A. S. Umar, V. E. Oberacker, and C. J. Horowitz, Microscopic sub-barrier fusion calculations for the neutron star crust, Phys. Rev. C **85**, 055801 (2012).

[94] C. Simenel, M. Dasgupta, D. J. Hinde, and E. Williams, Microscopic approach to coupled-channels effects on fusion, Phys. Rev. C **88**, 064604 (2013).

[95] A. S. Umar, C. Simenel, and V. E. Oberacker, Energy dependence of potential barriers and its effect on fusion cross sections, Phys. Rev. C **89**, 034611 (2014).

[96] X. Jiang, J. A. Maruhn, and S. Yan, Microscopic study of noncentral effects in heavy-ion fusion reactions with spherical nuclei, Phys. Rev. C **90**, 064618 (2014).

[97] S. E. Koonin, K. T. R. Davies, V. Maruhn-Rezwani, H. Feldmeier, S. J. Krieger, and J. W. Negele, Time-dependent Hartree-Fock calculations for ^{16}O + ^{16}O and ^{40}Ca + ^{40}Ca reactions, Phys. Rev. C **15**, 1359 (1977).

[98] C. Simenel, Particle Transfer Reactions with the Time-Dependent Hartree-Fock Theory Using a Particle Number Projection Technique, Phys. Rev. Lett. **105**, 192701 (2010).

[99] K. Sekizawa and K. Yabana, Time-dependent Hartree-Fock calculations for multinucleon transfer processes in ^{40,48}Ca + ^{124}Sn, ^{40}Ca + ^{208}Pb, and ^{58}Ni + ^{208}Pb reactions, Phys. Rev. C **88**, 014614 (2013).

[100] G. Scamps and D. Lacroix, Effect of pairing on one- and two-nucleon transfer below the Coulomb barrier: A time-dependent microscopic description, Phys. Rev. C **87**, 014605 (2013).

[101] K. Sekizawa and K. Yabana, Particle-number projection method in time-dependent Hartree-Fock theory: Properties of reaction products, Phys. Rev. C **90**, 064614 (2014).

[102] D. Bourgin, C. Simenel, S. Courtin, and F. Haas, Microscopic study of ^{40}Ca + ^{58,64}Ni fusion reactions, Phys. Rev. C **93**, 034604 (2016).

[103] C. Bottcher, M. R. Strayer, A. S. Umar, and P.-G. Reinhard, Damped relaxation techniques to calculate relativistic bound-states, Phys. Rev. A **40**, 4182 (1989).

[104] A. S. Umar and V. E. Oberacker, Three-dimensional unrestricted time-dependent Hartree-Fock fusion calculations using the full Skyrme interaction, Phys. Rev. C **73**, 054607 (2006).

[105] J. A. Maruhn, P.-G. Reinhard, P. D. Stevenson, and A. S. Umar, The TDHF code Sky3D, Comput. Phys. Commun. **185**, 2195 (2014).

[106] R. Balian and M. Vénéroni, Time-Dependent Variational Principle for Predicting the Expectation Value of an Observable, Phys. Rev. Lett. **47**, 1353 (1981).

[107] C. H. Dasso, T. Dossing, and H. C. Pauli, On the mass distribution in time-dependent Hartree-Fock calculations of heavy-ion collisions, Z. Phys. A **289**, 395 (1979).

[108] S. Ayik, A stochastic mean-field approach for nuclear dynamics, Phys. Lett. B **658**, 174 (2008).

[109] D. Lacroix and S. Ayik, Stochastic quantum dynamics beyond mean field, Eur. Phys. J. A **50**, 95 (2014).

[110] S. Ayik, O. Yilmaz, B. Yilmaz, and A. S. Umar, Quantal nucleon diffusion: Central collisions of symmetric nuclei, Phys. Rev. C **94**, 044624 (2016).

[111] S. Ayik, B. Yilmaz, O. Yilmaz, A. S. Umar, and G. Turan, Multinucleon transfer in central collisions of ^{238}U + ^{238}U, Phys. Rev. C **96**, 024611 (2017).

[112] S. Ayik, B. Yilmaz, O. Yilmaz, and A. S. Umar, Quantal diffusion description of multinucleon transfers in heavy-ion collisions, Phys. Rev. C **97**, 054618 (2018).

[113] S. Ayik, B. Yilmaz, O. Yilmaz, and A. S. Umar, Quantal diffusion approach for multinucleon transfers in Xe+Pb collisions, Phys. Rev. C **100**, 014609 (2019).

[114] S. Ayik, O. Yilmaz, B. Yilmaz, and A. S. Umar, Heavy-isotope production in ^{136}Xe + ^{208}Pb collisions at $E_{\mathrm{c.m.}} = 514$ MeV, Phys. Rev. C **100**, 044614 (2019).

[115] K.-H. Kim, Takaharu Otsuka, and Paul Bonche, Three-dimensional TDHF calculations for reactions of unstable nuclei, J. Phys. G **23**, 1267 (1997).

[116] A. S. Umar, M. R. Strayer, J. S. Wu, D. J. Dean, and M. C. Güçlü, Nuclear Hartree-Fock calculations with splines, Phys. Rev. C **44**, 2512 (1991).

[117] Y. Fu, H. Tong, X. F. Wang, H. Wang, D. Q. Wang, X. Y. Wang, and J. M. Yao, Microscopic analysis of shape transition in neutron-deficient Yb isotopes, Phys. Rev. C **97**, 014311 (2018).

[118] K. Nomura, T. Otsuka, R. Rodríguez-Guzmán, L. M. Robledo, and P. Sarriguren, Collective structural evolution in neutron-rich Yb, Hf, W, Os, and Pt isotopes, Phys. Rev. C **84**, 054316 (2011).

[119] L. M. Robledo, R. Rodríguez-Guzmán, and P. Sarriguren, Role of triaxiality in the ground-state shape of neutron-rich Yb, Hf, W, Os, and Pt isotopes, J. Phys. G **36**, 115104 (2009).

[120] P. Sarriguren, R. Rodríguez-Guzmán, and L. M. Robledo, Shape transitions in neutron-rich Yb, Hf, W, Os, and Pt

isotopes within a Skyrme Hartree-Fock + BCS approach, Phys. Rev. C **77**, 064322 (2008).

[121] C. Xu, H. Hua, X. Q. Li, J. Meng, Z. H. Li, F. R. Xu, Y. Shi, H. L. Liu, S. Q. Zhang, Z. Y. Li, L. H. Zhu, X. G. Wu, G. S. Li, C. Y. He, S. G. Zhou, S. Y. Wang, Y. L. Ye, D. X. Jiang, T. Zheng, J. L. Lou, L. Y. Ma, E. H. Wang, Y. Y. Cheng, and C. He, New insight into the shape coexistence and shape evolution of ^{157}Yb, Phys. Rev. C **83**, 014318 (2011).

[122] C. Simenel and B. Avez, Time–dependent Hartree–Fock description of heavy ions fusion, Int. J. Mod. Phys. E **17**, 31 (2008).

[123] C. Simenel, A. S. Umar, K. Godbey, M. Dasgupta, and D. J. Hinde, How the Pauli exclusion principle affects fusion of atomic nuclei, Phys. Rev. C **95**, 031601(R) (2017).

[124] W. Q. Shen, J. Albinski, A. Gobbi, S. Gralla, K. D. Hildenbrand, N. Herrmann, J. Kuzminski, W. F. J. Müller, H. Stelzer, J. Tõke, B. B. Back, S. Bjørnholm, and S. P. Sørensen, Fission and quasifission in U-induced reactions, Phys. Rev. C **36**, 115 (1987).

[125] D. J. Hinde, R. G. Thomas, R. du Rietz, A. Diaz-Torres, M. Dasgupta, M. L. Brown, M. Evers, L. R. Gasques, R. Rafiei, and M. D. Rodriguez, Disentangling Effects of Nuclear Structure in Heavy Element formation, Phys. Rev. Lett. **100**, 202701 (2008).

[126] C. Simenel, D. J. Hinde, R. du Rietz, M. Dasgupta, M. Evers, C. J. Lin, D. H. Luong, and A. Wakhle, Influence of entrance-channel magicity and isospin on quasi-fission, Phys. Lett. B **710**, 607 (2012).

[127] R. du Rietz, E. Williams, D. J. Hinde, M. Dasgupta, M. Evers, C. J. Lin, D. H. Luong, C. Simenel, and A. Wakhle, Mapping quasifission characteristics and timescales in heavy element formation reactions, Phys. Rev. C **88**, 054618 (2013).

[128] M. Morjean, D. J. Hinde, C. Simenel, D. Y. Jeung, M. Airiau, K. J. Cook, M. Dasgupta, A. Drouart, D. Jacquet, S. Kalkal, C. S. Palshetkar, E. Prasad, D. Rafferty, E. C. Simpson, L. Tassan-Got, K. Vo-Phuoc, and E. Williams, Evidence for the Role of Proton Shell Closure in Quasifission Reactions from X–Ray Fluorescence of Mass–Identified Fragments, Phys. Rev. Lett. **119**, 222502 (2017).

[129] G. Mohanto, D. J. Hinde, K. Banerjee, M. Dasgupta, D. Y. Jeung, C. Simenel, E. C. Simpson, A. Wakhle, E. Williams, I. P. Carter, K. J. Cook, D. H. Luong, C. S. Palshetkar, and D. C. Rafferty, Interplay of spherical closed shells and N/Z asymmetry in quasifission dynamics, Phys. Rev. C **97**, 054603 (2018).

[130] D. J. Hinde, D. Y. Jeung, E. Prasad, A. Wakhle, M. Dasgupta, M. Evers, D. H. Luong, R. du Rietz, C. Simenel, E. C. Simpson, and E. Williams, Sub–barrier quasifission in heavy element formation reactions with deformed actinide target nuclei, Phys. Rev. C **97**, 024616 (2018).

[131] K. Sekizawa and K. Yabana, Time-dependent Hartree-Fock calculations for multinucleon transfer and quasifission processes in the ^{64}Ni + ^{238}U reaction, Phys. Rev. C **93**, 054616 (2016).

[132] Edward Simpson, The Colourful Nuclide Chart, Technical Report (Australian National University, 2019).

[133] I. M. Itkis, E. M. Kozulin, M. G. Itkis, G. N. Knyazheva, A. A. Bogachev, E. V. Chernysheva, L. Krupa, Yu. Ts. Oganessian, V. I. Zagrebaev, A. Ya. Rusanov, F. Goennenwein, O. Dorvaux, L. Stuttgé, F. Hanappe, E. Vardaci, and E. de Goés Brennand, Fission and quasifission modes in heavy-ion-induced reactions leading to the formation of Hs*, Phys. Rev. C **83**, 064613 (2011).

[134] M. G. Itkis, E. Vardaci, I. M. Itkis, G. N. Knyazheva, and E. M. Kozulin, Fusion and fission of heavy and superheavy nuclei (experiment), Nucl. Phys. A **944**, 204 (2015).

[135] E. M. Kozulin, G. N. Knyazheva, T. K. Ghosh, A. Sen, I. M. Itkis, M. G. Itkis, K. V. Novikov, I. N. Diatlov, I. V. Pchelintsev, C. Bhattacharya, S. Bhattacharya, K. Banerjee, E. O. Saveleva, and I. V. Vorobiev, Fission and quasifission of the composite system Z = 114 formed in heavy-ion reactions at energies near the Coulomb barrier, Phys. Rev. C **99**, 014616 (2019).

[136] K. Banerjee, D. J. Hinde, M. Dasgupta, E. C. Simpson, D. Y. Jeung, C. Simenel, B. M. A. Swinton-Bland, E. Williams, I. P. Carter, K. J. Cook, H. M. David, C. E. Düllmann, J. Khuyagbaatar, B. Kindler, B. Lommel, E. Prasad, C. Sengupta, J. F. Smith, K. Vo-Phuoc, J. Walshe, and A. Yakushev, Mechanisms Suppressing Superheavy Element Yields in Cold Fusion Reactions, Phys. Rev. Lett. **122**, 232503 (2019).

[137] R. G. Thomas, D. J. Hinde, D. Duniec, F. Zenke, M. Dasgupta, M. L. Brown, M. Evers, L. R. Gasques, M. D. Rodriguez, and A. Diaz-Torres, Entrance channel dependence of quasifission in reactions forming ^{220}Th, Phys. Rev. C **77**, 034610 (2008).

[138] K. Sekizawa, Microscopic description of production cross sections including deexcitation effects, Phys. Rev. C **96**, 014615 (2017).

[139] A. Bulgac, S. Jin, and I. Stetcu, Unitary evolution with fluctuations and dissipation, Phys. Rev. C **100**, 014615 (2019).